Rapid Communications | Editors' Suggestion

Ultrafast quantum-path interferometry revealing the generation process of coherent phonons

Kazutaka G. Nakamura,[1,*] Kensuke Yokota,[1] Yuki Okuda,[1] Rintaro Kase,[1] Takashi Kitashima,[1] Yu Mishima,[1] Yutaka Shikano,[2,3,4,5] and Yosuke Kayanuma[1,6,†]

[1]*Laboratory for Materials and Structures, Institute of Innovative Research, Tokyo Institute of Technology, 4259 Nagatsuta, Yokohama 226-8503, Japan*

[2]*Quantum Computing Center, Keio University, 3-14-1 Gakuen-cho, Yokohama 223-8522, Japan*

[3]*Research Center for Advanced Science and Technology (RCAST), The University of Tokyo, 4-6-1 Komaba, Meguro, Tokyo 153-8904, Japan*

[4]*Research Center of Integrative Molecular Systems (CIMoS), Institute for Molecular Science, National Institutes of Natural Sciences, 38 Nishigo-Naka, Myodaiji, Okazaki, Aichi 444-8585, Japan*

[5]*Institute for Quantum Studies, Chapman University, 1 University Dr., Orange, California 92866, USA*

[6]*Graduate School of Sciences, Osaka Prefecture University, 1-1 Gakuen-cho, Sakai, Osaka 599-8531, Japan*

(Received 21 November 2018; revised manuscript received 18 March 2019; published 20 May 2019)

Optical dual-pulse pumping actively creates quantum-mechanical superposition of the electronic and phononic states in a bulk solid. We here made transient reflectivity measurements in an *n*-GaAs using a pair of relative-phase-locked femtosecond pulses and found characteristic interference fringes. This is a result of quantum-path interference peculiar to the dual-pulse excitation as indicated by theoretical calculation. Our observation reveals that the pathway of coherent phonon generation in the *n*-GaAs is impulsive stimulated Raman scattering at the displaced potential due to the surface-charge field, even though the photon energy lies in the opaque region.

DOI: 10.1103/PhysRevB.99.180301

Coherent control is a technique of manipulating quantum states in materials using optical pulses [1–3]. A wave packet in quantum-mechanical superposition is created by the optical pulse via several quantum transition paths. In the case of a double-pulse excitation, wave packets created by transitions in each pulse and across the two pulses interfere and the generated superposition state is manipulated by controlling a delay between the two pulses [4,5]. A contribution of individual quantum paths can be extracted from the interference pattern, which is referred to as quantum-path interferometry [6].

Coherent phonons are a temporally coherent oscillation of the optical phonons induced by the impulsive excitation of an ultrashort optical pulse [7–12]. Using coherent phonons and making a pump-probe-type optical measurement, we can directly observe the dynamics of the electron-phonon coupled states in the time domain for a wide variety of materials [13–26]. In this respect, the clarification of the generation mechanism of the coherent phonon is a fundamental subject as an ultrafast dynamical process [18,27–29]. The generation mechanisms of coherent phonons are usually categorized as two types: a mechanism of impulsive stimulated Raman scattering (ISRS) [7] and a mechanism of displaced enhanced coherent phonons [13]. In addition, for polar semiconductors such as GaAs, the screening of the surface-space-charge field [16,27] is considered to be another generation mechanism for opaque conditions. The generation mechanism of coherent phonons may become a controversial subject in the case of opaque-region pumping because impulsive absorption (IA) and ISRS processes coexist as possible quantum-mechanical transition paths [30]. A novel experimental technique is needed to shed light on this subject.

In the present work, we apply quantum-path interferometry to study the generation process of coherent optical phonons through the coherent control of electron-phonon coupled states in bulk solids. Coherent phonons are often coherently controlled using a pair of femtosecond pulses as pump pulses, and the phonon amplitude is enhanced or suppressed via the constructive or destructive interference of induced phonons [15,31]. Unlike these earlier works, we used two relative-phase-locked pump pulses (pulses 1 and 2) and a delayed probe pulse (pulse 3) [32], for quantum-path interferometry. If the delay of the dual-pump pulses t_{12} was controlled with subfemtosecond accuracy and if the electronic coherence was maintained during the dual pulses, electronic excited states were created as a quantum-mechanical superposition; i.e., the electronic polarizations induced by pulses 1 and 2 interfered with each other. Meanwhile, polarization in the phonon system was coherently created with resulting interference within the phononic and electronic degrees of freedom. The probe pulse was used to monitor the interference fringe via heterodyne detection; i.e., via a change in the reflectivity as a function of the pump-pump delay t_{12} and pump-probe delay t_{13}. We could evaluate the electronic and phononic coherence times of the sample using this scheme. Furthermore, a theoretical estimation predicts a decisive difference in the interference fringes between ISRS and IA, and it will be shown that the dominant pathway of the generation of coherent phonons can be determined from the pump-pulse-delay-dependent interference pattern of generation efficiency.

A femtosecond optical pulse (central wavelength of 798 nm, pulse width of ∼50 fs) was split with a partial beam splitter into two pulses (i.e., pump and probe pulses). The

*Corresponding author: nakamura@msl.titech.ac.jp
†kayanuma.y.aa@m.titech.ac.jp

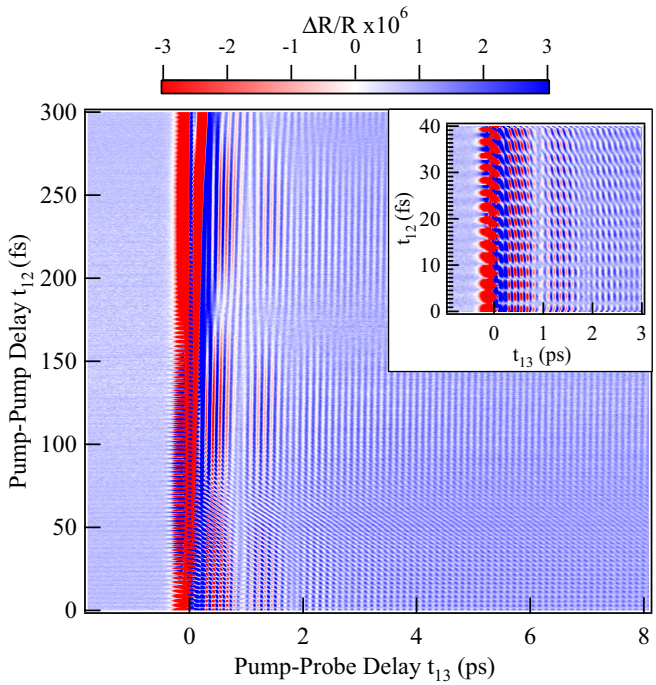

FIG. 1. Two-dimensional image map of the change in reflection intensity with the pump-probe delay (t_{13}) and pump-pump delay (t_{12}).

pump pulse was introduced into a homemade Michelson-type interferometer to produce relative-phase-locked pump pulses (i.e., pulses 1 and 2), in which stability was within ±6%. The probe pulse (i.e., pulse 3) was irradiated with a controlled time delay. The optical bandpass filter (the center wavelength of 800 nm with the bandwidth of 10 nm) was used for detecting the reflected probe pulse in order to reduce cancellation effects of Stokes and anti-Stokes components [33]. We set the two pump pulses in a collinear condition with parallel polarization in the present experiments. The k-vector direction of the two interfering pump pulses may affect the interference fringes. The sample was a single crystal of n-GaAs with (100) orientation and kept at 90 K in a cryostat. Details of the experimental setting are described in the Supplemental Material [34].

Figure 1 is a two-dimensional map of the transient reflectivity change $\Delta R/R$ plotted against the pump-probe delay t_{13} and pump-pump delay t_{12}. For a fixed value of t_{12}, $\Delta R/R$ indicates an oscillation with periods of 115 and 128 fs, which are equal to the periods of the longitudinal-optical (LO) phonon and LO phonon-plasmon coupled mode (LOPC) at the Γ point in GaAs [35–38]. For a fixed value of t_{13}, meanwhile, $\Delta R/R$ has a beat between a rapid oscillation with a period of 2.7 fs, which is nearly equal to that of the pump laser with a wavelength of 798 nm, and a slow oscillation with vibration periods of the LO phonon and LOPC.

For fixed values of t_{12}, a Fourier transformation of the signal $\Delta R/R$ was carried out with respect to t_{13}. The Fourier transformation was performed over the interval of 0.25 ps $< t_{13} <$ 2.25 ps after the irradiation of pump 2 to avoid the spurious effect of excess charge in the very early stage and the effect of phonon decay at a late time. Figure 2 is a plot of the oscillation amplitude ΔR^0 of the Fourier-transformed data against the frequency ω_{13} and delay t_{12}. The figure shows

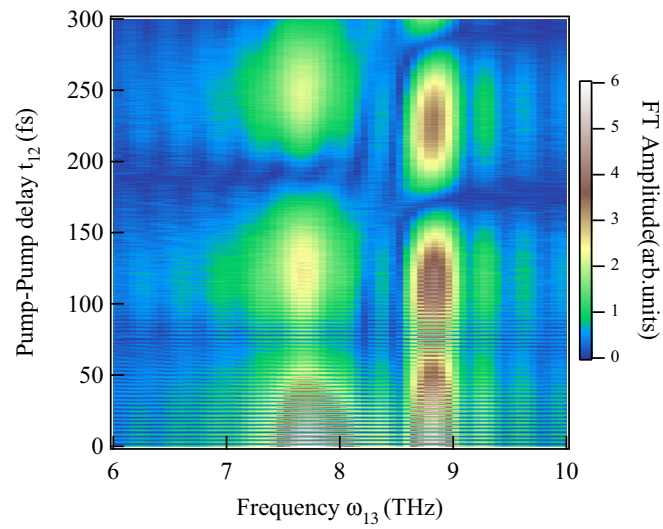

FIG. 2. Two-dimensional image map of the Fourier spectra at various pump-probe delays (t_{13}).

that two modes of coherent oscillations are excited in the crystal.

To see more clearly the t_{12} dependence of the oscillation amplitude ΔR^0 of the transient reflectivity, we plotted ΔR^0 at peak values at frequency ω_{13} of 8.7 and 7.8 THz for the LO and LOPC modes, respectively. Figure 3(a) presents results for the LO mode. The LOPC mode shown in Fig. 3(b) has qualitatively the same interference pattern as the LO mode.

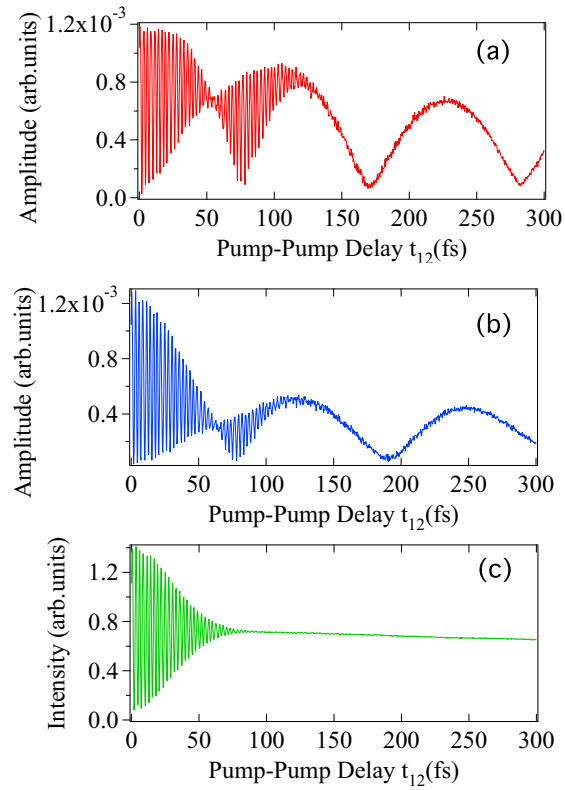

FIG. 3. Interference fringe of LO phonon (a) and LOPC (b) and optical interference (c).

In Fig. 3(a), the rapid oscillation with a period of ∼2.7 fs is the interference fringe of the electronic states that memorized the phase of the pump-laser field. The slow oscillation with period ∼115 fs is the interference fringe due to the coherence of phonons. The rapid interference fringes disappeared when we used the cross-polarized pump pulses.

Note that the electronic coherence survives well after the overlapping of the pump pulses ends, as can be seen from comparison with the linear optical interference of the dual pulses [Fig. 3(c)]. This means that the optical phase of pulse 1 is imprinted on the electronic polarization and interferes with that of pulse 2. The most important feature of the interference pattern is the apparent collapse and revival of the electronic fringe at around $t_{12} \sim 55$ fs. It will be shown below that this is due to a quantum-path interference peculiar to the ISRS process.

In the time region where t_{13} is large enough compared with t_{12} and the pulse width, it is safely assumed that the generation process and the detection process of coherent phonons are well separated. Hereafter, we concentrate on the generation process of LO phonons. See Supplemental Material [34] for the theoretical treatment of the probe processes. For microscopic interactions that induce the coherent oscillation of LO phonons through the irradiation of ultrashort optical pulses, several models are conceivable, including the Fröhlich interaction [39] and deformation-potential interaction [40]. In the case of polar materials, it is considered that electrostatic interaction due to transient depletion field screening plays a central role [27]. It is known that there are two types of photoinduced current: the usual injection current following the real excitation of carriers and the shift current resulting from quantum-mechanical polarization induced by optical pulses [42,43], in ionic semiconductors [41]. The response of the shift current is usually faster than that of the injection current.

We assume a model Hamiltonian that describes the electron-phonon interaction as

$$H = \{\epsilon_g + \hbar\omega b^\dagger b\}|g\rangle\langle g| + \sum_k \{\epsilon_k + \hbar\omega b^\dagger b + \alpha\hbar\omega(b + b^\dagger)\}|k\rangle\langle k|, \quad (1)$$

where $|g\rangle$ is the electronic ground state of the crystal with energy ϵ_g and $|k\rangle$ the excited state with energy ϵ_k. The creation and annihilation operators of the LO phonon at the Γ point with energy $\hbar\omega$ are respectively denoted $b^\dagger$ and b. It is assumed that the dimensionless electron-phonon coupling constant α is small and k independent, assuming a rigid-band shift. The parameter α indicates the displacement of the potential, where all effects on deformation of the potential, such as the surface-space-charge field, are included. See the Supplemental Material [34] for a detailed explanation.

Within the rotating-wave approximation, the interaction Hamiltonian with a dual-pump pulse is given by

$$H_{\rm pump}(t) = E_{pu}(t)\sum_k \mu_k|k\rangle\langle g| + \text{H.c.}, \quad (2)$$

where μ_k is the transition dipole moment from $|g\rangle$ to $|k\rangle$. $E_{pu}(t)$ is the temporal profile of the electric field of the pump pulse,

$$E_{pu}(t) = E_0[f(t)e^{-i\Omega_0 t} + f(t - t_{12})e^{-i\Omega_0(t-t_{12})}], \quad (3)$$

where Ω_0 is the carrier frequency of the laser pulse.

Here, $f(t)$ is the pulse envelope, which is assumed to have a Gaussian form, $f(t) = (1/\sqrt{\pi}\sigma\Omega_0)e^{-t^2/\sigma^2}$, and E_0 is the amplitude of the electric field. A fundamental quantity used to describe the optical properties of crystals is the electric response function given by

$$F(t) = \sum_k |\mu_k|^2 e^{-i(\epsilon_k - \epsilon_g)t/\hbar - \eta|t|/\hbar} \quad (\eta = 0_+), \quad (4)$$

which is obtained via the Fourier transform of the effective optical absorption spectrum $I_{\rm eff}(\Omega)$.

We adopt the density matrix formalism to derive the generation amplitude of the coherent phonon. The change of the amplitude ΔR of the reflectivity is proportional to the expectation value of the LO phonon coordinate $Q = \sqrt{\hbar/2\omega}(b + b^\dagger)$ except for constant factors. See Supplemental Material [34] for the formula of spectrally resolved detection of reflectivity modulation. Figure 4 presents double-sided Feynman diagrams for the generation by ISRS [Fig. 4(a)] and IA [Fig. 4(b)]. In Fig. 4, the propagators shown by

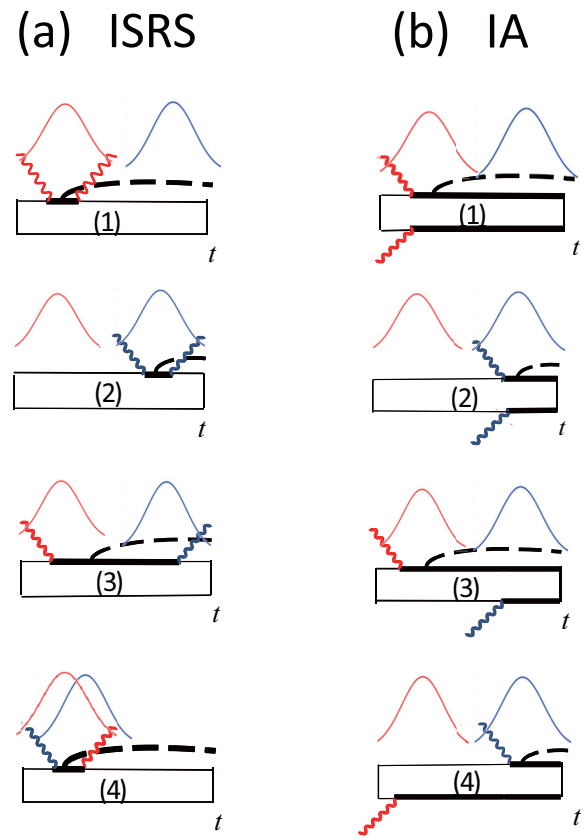

FIG. 4. Double-sided Feynman diagrams for the density matrices corresponding to (a) the ISRS process and (b) the IA process. The thin and thick solid lines respectively represent the ground and excited states. The dashed curves represent the one-LO-phonon state. The red and blue Gaussian curves represent the pulse envelope of the first and the second pulses, respectively, with the wavy lines their photon propagators.

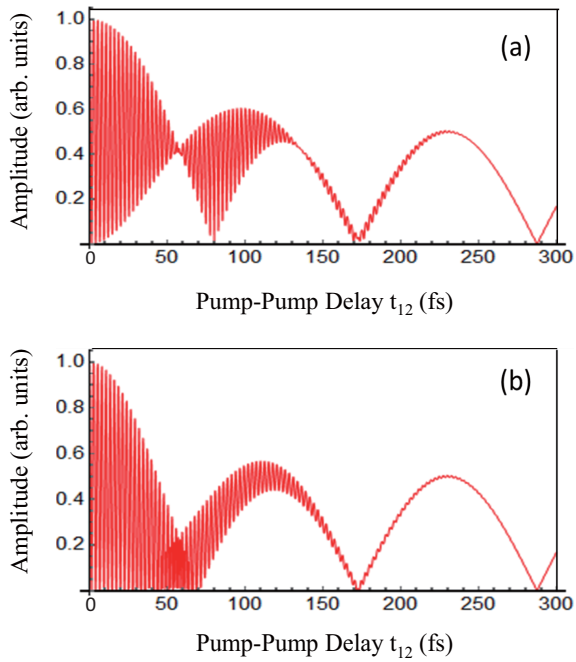

FIG. 5. (a) Theoretical curve for the interference fringe in the oscillation amplitude of transient reflectivity due to the ISRS process at the LO phonon frequency plotted against the pump-pump delay (t_{12}). (b) Same as (a) but for the IA process.

thin lines correspond to the ground state and those shown by bold lines correspond to the excited state. The dashed lines represent the one-phonon state. Note that the Hermitian conjugate terms arise from the processes in the diagrams in which the upper and the lower propagators are interchanged, but these processes are ignored in Fig. 4(a) for simplicity.

After a perturbation calculation, the amplitude of the oscillation of coherent phonons in the ISRS and IA processes, $A_{\rm ISRS}$ and $A_{\rm IA}$ are respectively given as

$$A_i(t_{12}) = L_i(0) + e^{i\omega t_{12}} L_i(0) + e^{-i[\Omega_0-(\omega/2)]t_{12}} L_i(t_{12}) + e^{i[\Omega_0+(\omega/2)]t_{12}} L_i(-t_{12}), \quad (5)$$

in which $i =$ ISRS, IA and

$$L_{\rm ISRS}(x) = 2i \int_0^\infty du\, g(u-x) \sin\frac{\omega u}{2} e^{i\Omega_0 u} F(u), \quad (6)$$

$$L_{\rm IA}(x) = \int_{-\infty}^{\infty} du\, g(u-x) e^{i[\Omega_0-(\omega/2)]u} F(u), \quad (7)$$

with $g(u) = e^{-u^2/(2\sigma^2)}$, $x = 0, t_{12}, -t_{12}$. The amplitude $\Delta R^{(0)}$ is proportional to the absolute values of $A_i(t_{12})$. The first, second, third, and fourth terms in Eq. (5) correspond to the processes (1)–(4) in Fig. 4, respectively. Details of the calculation are shown in the Supplemental Material [34].

The actual calculation of the transient reflectivity can be done for real materials if the electric response function $F(t)$ is given. In the calculation, we assumed a Lorentzian form, $I_{\rm eff}(\Omega) = I_0(\Gamma/\pi)/\{(\Omega-\Omega_0)^2+\Gamma^2\}$, with $\hbar\Omega_0 = 1.55$ eV and $\Gamma = 0.015$ eV based on the absorption spectra [44,45]. The calculated fringe patterns ΔR^0 are shown for ISRS [Fig. 5(a)] and IA [Fig. 5(b)]. We found that the features in the fringe shown in Fig. 3(a) are well reproduced if it is assumed that only the ISRS process contributes to the generation of coherent phonons. Furthermore, the overall line shape is in good agreement with experimental data.

Most important is the fact that the feature of the collapse and revival of the electronic fringe at around $t_{12} \sim 55$ fs arises only from the ISRS process, while the IA signal does not yield any such feature. This is due to the quantum-path interference peculiar to ISRS. In Fig. 4(a), the contribution arising from diagrams (1) and (2) gives rise only to the interference of the phonon, which is described by the first and second terms on the right-hand side of Eq. (5). The electronic interference arises from diagrams (3) and (4), which correspond to the third and fourth terms, respectively, in Eq. (5). It should be noted that the fourth term in $A_{\rm ISRS}(t_{12})$ is negligibly small for $t_{12} > 0$. Therefore, in ISRS, the electronic interference fringe appears only from the cross term between (1) + (2) and (3). At $t_{12} = \pi/\omega$, this term vanishes owing to the destructive interference of the phonon. The high-frequency oscillation of the electronic fringe therefore disappears at $t_{12} = \pi/\omega =$ 55 fs. This is a manifestation of the path interference of the electronic and phononic degrees of freedom in the dual-pump process peculiar to the ISRS. Note that in the IA process, both the third and fourth terms in $A_{\rm IA}(t_{12})$ make a finite contribution so that the electronic fringe does not vanish at $t_{12} = \pi/\omega$.

In Fig. 5(a), the amplitude of the electronic fringe becomes small for $t_{12} > 130$ fs. This is due to the dephasing caused by the inhomogeneous broadening of the continuous spectrum in the excited states. In the experimental curve in Fig. 3(a), the electronic fringe disappears almost completely for $t_{12} >$ 130 fs in contrast to the case in Fig. 5.

The finding of the ISRS dominance in coherent phonon generation in the opaque region is surprising because, in the opaque region, the phonon generation intensity in the IA process is generally estimated to be higher than that for ISRS [29,30,46]. We conjecture that even if the coherent phonon may be generated in the excited state subspace, its coherence is quickly lost because of the ultrafast deformation of the adiabatic potentials due to the electronic relaxation in the excited state of bulk materials. This may be one of the differences in the atomic and molecular dynamics of solids compared with those of the gas phase, in which the excited electronic states are long protected from relaxation. In addition, it was revealed that the generation of the coherent phonon in GaAs is a quick process as deduced from ISRS dominance even in the opaque region. The underlying mechanism is the quantum mechanically induced shift current.

In summary, we made transient reflectivity measurements for *n*-GaAs using relative-phase-locked femtosecond pulses and found characteristic interference fringes, which are assigned to quantum-path interference in the generation of coherent phonons. Our observations and theory revealed that the pathway of coherent phonon generation in *n*-GaAs is ISRS at the displaced potential due to the surface-charge field, even though the photon energy lies in the opaque region. We demonstrated that optical dual-pulse pumping actively creates quantum-mechanical superposition of the electronic and phononic states in a bulk solid.

The authors thank K. Norimatsu, K. Goto, H. Matsumoto, and F. Minami for their help with the experiments and calculation. K.G.N., Y.S., and Y.K. thank K. Ohmori, H. Chiba, H. Katsuki, and Y. Okano of the Institute of Molecular Science for their valuable advice on the experiments. This work was partially supported by Core Research for Evolutional Science and Technology of the Japan Science and Technology Agency, JSPS KAKENHI under Grants No. 25400330, No. 14J11318, No. 15K13377, No. 16K05396, No. 16K05410, No. 17K19051, and No. 17H02797, the Collaborative Research Project of Laboratory for Materials and Structures, the Joint Studies Program of the Institute of Molecular Science, National Institutes of Natural Sciences, and The Precise Measurement Technology Promotion Foundation.

[1] P. Brumer and M. Shapiro, Chem. Phys. Lett. **126**, 541 (1986).
[2] S. A. Rice, D. J. Tannor, and R. Kosloff, J. Chem. Soc., Faraday Trans. **82**, 2423 (1986).
[3] N. F. Scherer, R. J. Carlson, A. Matro, M. Du, A. J. Ruggiero, V. Romero-Rochin, J. A. Cina, G. R. Fleming, and S. A. Rice, J. Chem. Phys. **95**, 1487 (1991).
[4] H. Katsuki, N. Takei, C. Sommer, and K. Ohmori, Acc. Chem. Res. **51**, 1174 (2018).
[5] H. Mashiko, Y. Chisuga, I. Katayama, K. Oguri, H. Masuda, J. Takeda, and H. Gotoh, Nat. Commun. **9**, 1468 (2018).
[6] D. R. Austin and I. A. Walmsley, in *CLEO/Europe and EQEC 2011 Conference Digest*, OSA Technical Digest (CD) (Optical Society of America, 2011).
[7] Y.-X. Yan, E. B. Gamble, and K. Nelson, J. Chem. Phys. **83**, 5391 (1985).
[8] R. Merlin, Solid State Commun. **102**, 207 (1997).
[9] T. Dekorsy, G. C. Cho, and H. Kurz, in *Light Scattering in Solids III*, edited by M. Cardona and G. Güntherodt (Springer, Berlin, 2000), pp. 169–209.
[10] O. V. Misochko, J. Exp. Theor. Phys. **92**, 246 (2001).
[11] F. Randi, M. Esposito, F. Giusti, O. Misochko, F. Parmigiani, D. Fausti, and M. Eckstein, Phys. Rev. Lett. **119**, 187403 (2017).
[12] F. Glerean, S. Marcantoni, G. Sparapassi, A. Blason, M. Esposito, F. Benatti, and D. Fausti, J. Phys. B: At. Mol. Opt. Phys., doi: 10.1088/1361-6455/ab0bdc
[13] H. J. Zeiger, J. Vidal, T. K. Cheng, E. P. Ippen, G. Dresselhaus, and M. S. Dresselhaus, Phys. Rev. B **45**, 768 (1992).
[14] M. F. DeCamp, D. A. Reis, P. H. Bucksbaum, and R. Merlin, Phys. Rev. B **64**, 092301 (2001).
[15] H. Katsuki, J. C. Delagnes, K. Hosaka, K. Ishioka, H. Chiba, E. S. Zijlstra, M. E. Garcia, H. Takahashi, K. Watanabe, M. Kitajima, Y. Matsumoto, K. G. Nakamura, and K. Ohmori, Nat. Commun. **4**, 2801 (2013).
[16] G. C. Cho, W. Kütt, and H. Kurz, Phys. Rev. Lett. **65**, 764 (1990).
[17] T. Dekorsy, T. Pfeifer, W. Kütt, and H. Kurz, Phys. Rev. B **47**, 3842 (1993).
[18] G. A. Garrett, T. F. Albrecht, J. F. Whitaker, and R. Merlin, Phys. Rev. Lett. **77**, 3661 (1996).
[19] O. V. Misochko, K. Kisoda, K. Sakai, and S. Nakashima, Phys. Rev. B **61**, 4305 (2000).
[20] M. Hase, M. Kitajima, A. M. Constantinescu, and H. Petek, Nature (London) **426**, 51 (2003).
[21] A. Q. Wu, X. Xu, and R. Venkatasubramanian, Appl. Phys. Lett. **92**, 011108 (2008).
[22] N. Kamaraju, S. Kumar, and A. K. Sood, Europhys. Lett. **92**, 47007 (2010).
[23] K. Norimatsu, J. Hu, A. Goto, K. Igarashi, T. Sasagawa, and K. G. Nakamura, Solid State Commun. **157**, 58 (2013).
[24] O. V. Misochko, J. Flock, and T. Dekorsy, Phys. Rev. B **91**, 174303 (2015).
[25] D. M. Riffe and A. J. Sabbah, Phys. Rev. B **76**, 085207 (2007).
[26] F. Sun, Q. Wu, Y. L. Wu, H. Zhao, C. J. Yi, Y. C. Tian, H. W. Liu, Y. G. Shi, H. Ding, X. Dai, P. Richard, and J. Zhao, Phys. Rev. B **95**, 235108 (2017).
[27] T. Pfeifer, T. Dekorsy, W. Kütt, and H. Kurz, Appl. Phys. A **55**, 482 (1992).
[28] A. V. Kuznetsov and C. J. Stanton, Phys. Rev. B **51**, 7555 (1995).
[29] T. E. Stevens, J. Kuhl, and R. Merlin, Phys. Rev. B **65**, 144304 (2002).
[30] K. G. Nakamura, Y. Shikano, and Y. Kayanuma, Phys. Rev. B **92**, 144304 (2015).
[31] M. Hase, M. Mizoguchi, H. Harima, S. Nakashima, M. Tani, K. Sakai, and M. Hangyo, Appl. Phys. Lett. **69**, 2474 (1996).
[32] S. Hayashi, K. Kato, K. Norimatsu, M. Hada, Y. Kayanuma, and K. G. Nakamura, Sci. Rep. **4**, 4456 (2014).
[33] K. G. Nakamura, K. Ohya, H. Takahashi, T. Tsuruta, H. Sasaki, S.-I. Uozumi, K. Norimatsu, M. Kitajima, Y. Shikano, and Y. Kayanuma, Phys. Rev. B **94**, 024303 (2016).
[34] See Supplemental Material at http://link.aps.org/supplemental/10.1103/PhysRevB.99.180301 for the details of experimental setup and sample, deformed harmonic potential, and details of the calculation of coherent phonon generation and spectrally resolved detection.
[35] A. Mooradian and A. L. McWhorter, Phys. Rev. Lett. **19**, 849 (1967).
[36] J. D. Lee and M. Hase, Phys. Rev. Lett. **101**, 235501 (2008).
[37] K. Ishioka, A. K. Basak, and H. Petek, Phys. Rev. B **84**, 235202 (2011).
[38] J. Hu, O. V. Misochko, A. Goto, and K. G. Nakamura, Phys. Rev. B **86**, 235145 (2012).
[39] H. Fröhlich, Adv. Phys. **3**, 325 (1954).
[40] Y. R. Shen and N. Bloembergen, Phys. Rev. **137**, A1787 (1965).
[41] F. Nastos and J. E. Sipe, Phys. Rev. B **74**, 035201 (2006).
[42] J. E. Sipe and A. I. Shkrebtii, Phys. Rev. B **61**, 5337 (2000).
[43] A. V. Kuznetsov and C. J. Stanton, Phys. Rev. B **48**, 10828 (1993).
[44] M. D. Sturge, Phys. Rev. **127**, 768 (1962).
[45] H. C. Casey, Jr., D. D. Sell, and K. W. Wecht, J. Appl. Phys. **46**, 250 (1974).
[46] Y. Kayanuma and K. G. Nakamura, Phys. Rev. B **95**, 104302 (2017).